I&EC research
Industrial & Engineering Chemistry Research

pubs.acs.org/IECR

Article

Supercritical Fluid Extraction of the Seed Fatty Oil: Sensitivity to the Solute Axial Dispersion

Artur A. Salamatin*

Cite This: https://dx.doi.org/10.1021/acs.iecr.0c03329

Read Online

ACCESS | Metrics & More | Article Recommendations | Supporting Information

ABSTRACT: Successful development of an industrial-scale process for supercritical fluid extraction (SFE) of oil from ground plant material requires detailed analysis of the effects associated with the solute transport in porous media. In the present paper, a case of the raw material with high initial oil content is considered, and the influence of the axial flow dispersion on the extraction dynamics is analyzed numerically and analytically. The typical one-dimensional convection−dispersion mass-transfer model on the extractor-scale level is revisited, and the widely accepted shrinking core model is used to describe the solute diffusion on the particle-scale level. The SFE description also accounts for the polydispersity of the ground material. The set of dimensionless parameters required for complete analysis of different extraction regimes is defined. The influence of the axial flow dispersion on the extraction kinetics manifests itself mainly via polydispersity of the ground raw material, despite being insignificant in typical SFE implementations.

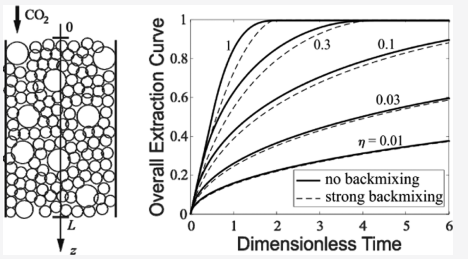

1. INTRODUCTION

The process of supercritical fluid extraction (SFE) employs fluids (solvents) at temperatures and pressures above or near the corresponding critical values. Carbon dioxide (CO_2) is one of the most commonly used solvents because it is environmentally friendly, nontoxic, has a moderate critical temperature, ∼31 °C, and can be easily separated from the extract by reducing the pressure. The new technology is widely used in pharmaceutical production and in the food and biofuel industry.[1,2] The extraction of natural compounds from plant matrices (ground seeds, leaves, petals, etc.) remains one of the most common applications of the SFE process.[3,4] Particularly, sunflower,[5,6] rape,[7] pumpkin seeds,[8] apricot kernels,[9] etc. with high oil contents are sources of valuable natural compounds.

The extraction takes place in a cylindrical vessel (extraction column), where particles of ground raw material are placed to form a porous packed bed (Figure 1). The solvent is injected initially into the vessel until the operational pressure (40−70 MPa) and temperature (40−70 °C) are reached. The fluid penetrates the oil-containing cells of the plant material and dissolves the extractable oil components. Then, the solvent is pumped through the bed at a given flow rate under the applied pressure gradient. During the extraction process, the solute diffuses along the internal transport channels inside the plant particles[10−13] to the surface of the ground material and is transported further by the fluid flow to the outlet cross section of the vessel. The oil concentration gradient along the individual particles is the driving force of extraction.

Mass transfer in packed beds under flow conditions is subject to dispersion, particularly in the axial, z-direction. This macroscopic effect, caused by spatial inhomogeneity of the bed porosity, fluid velocity, and its properties (due to temperature and pressure gradients), etc., can significantly reduce extraction rates. The maximum driving force of mass transfer at minimum dispersion is of primary interest in industrial-scale operations. Certain approaches, in particular, the regime of enhanced solvent consumption, have already been proposed to suppress the axial dispersion during SFE in cylindrical vessels.[1,14] However, this decreases the time the fluid spends in the bed and results in an increase of the net production costs. Thus, the interaction between the solvent flow rates and dispersive transport impact should be investigated to find the optimal tradeoff.

Elaborate SFE models pave the way toward understanding the principal mechanisms controlling the extraction and allow for the theoretical search of optimal extraction conditions[13,15−19] at minimum overall costs of technology development.

The detailed micro-scale picture of solvent flows in packed beds of polydisperse particles is highly irregular and random, and for practical applications, the mass-transfer phenomena are conventionally described and studied on the macro-scale level within the framework of spatial (volumetric) averaging[20−24] in terms of the macroscopic characteristics. The above-mentioned micro-scale inhomogeneities of the mass-transfer phenomena in porous media manifest themselves as apparent dispersion effects, i.e., apparent diffusivity, in averaging procedures, in

Received: July 6, 2020
Revised: September 8, 2020
Accepted: September 10, 2020
Published: September 10, 2020

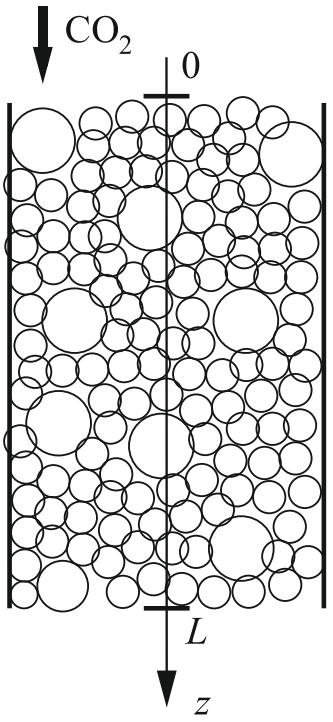

Figure 1. Vertical cross section of a packed bed of polydisperse spherical particles of ground raw material. Two sizes of particles are shown. The supercritical CO_2 flows from the top to the bottom of the column, along the z-direction. The height of the packed bed is L.

macro-scale models used to calculate the average concentration of solute in the packed bed under flow conditions.[25]

The approach to SFE modeling accounts for the microscopic mass-transfer phenomena, which include solute transport in particles of raw material and across the diffusive boundary layer formed at large Peclet numbers[26−30] on the particle surface, as well as the macroscopic phenomena, which include dispersion in the bulk flow.[22,25,31−35] Therefore, additional closing relations are needed to complete the macro-scale-level problem formulation.

Two models for the detailed, internal mass transfer in particles, shrinking core (SC)[6,13,19] and broken-and-intact cells (BIC),[36−38] are in present-day use, and the SC model is employed here in Section 2.1. The model allows for the explicit account of the polydispersity of the ground material and has been recently validated on a representative set of data.[19,39]

Importantly, the molecular diffusion coefficient in the fluid phase is three to four orders of magnitude larger than the apparent diffusion coefficient in the raw material,[19] and the diffusion through the boundary layer is even faster compared to that in particles. Estimates of the Sherwood number based on available empirical[40−43] and theoretical correlations[29,30,44] suggest that the particle mass-transfer coefficient is $\sim 10^{-6}$ to 10^{-5} m·s^{-1} and the Peclet number is on the order of $\sim 10-10^4$. Thus, the corresponding mass-transfer Biot number is large, $\sim 10^4$ to 10^5, and the resistance of the boundary layer is hereinafter neglected in accordance with Goto et al.[13] More details are given in the Supporting Information.

The commonly applied phenomenological description of the mass transfer in packed beds is introduced in Section 2.2. For the case of an isotropic porous medium, the dispersion tensor has only diagonal nonzero components, and the longitudinal (or axial) dispersion coefficient D_{ax} that controls the solute distribution along the averaged (macro-scale) flow in the z-direction is of primary interest. The other two so-called lateral (or transversal) dispersion coefficients contribute to the radial spread of the solute[24,25] and do not enter the macroscopic mass transfer equations in a one-dimensional approximation of the solvent flow.

In general, closing relations for the dispersion coefficient are given in the form of empirical (or analytical) correlations for the D_{ax} dependence on macroscopic parameters, such as solvent flow rate, packed bed porosity, polydispersity, particle diameter to vessel diameter, vessel diameter-to-height ratios, etc. As a rule, available data for supercritical conditions are limited to laboratory experiments with inert monodisperse particles without mass exchange between phases, i.e., passive dispersion. Such conditions dominate in experimental studies.[34,45−48] However, solute interacts with the solid phase under SFE conditions, and the available correlations cannot be directly applied to systems with heterogeneous reactions, i.e., systems with active dispersion, since the dispersion tensor depends on extraction (heterogeneous reaction) parameters.[1,20,35]

Preliminary analysis and comparison of various mass-transfer regimes are required to estimate possible errors related to the dispersion coefficient uncertainties. Obviously, the entire spectrum of the extraction mass-transfer regimes falls between the case of the plug flow, $D_{ax} \to 0$, and the ideal-mixer regime, $D_{ax} \to \infty$.

The aim of the present study is to undertake sensitivity tests of the validated SFE model (Section 2.2) and investigate theoretically the influence of the axial dispersion on the SFE effectiveness, in particular extraction rates, with respect to the height of the packed bed, solvent consumption rates, characteristic particle size, particle size distribution, and other conditions. The axial dispersion coefficient D_{ax} is varied independently of other process parameters, and the available correlations are used to introduce the reference values for discussion. Thus, the analysis covers the whole spectrum of regimes under SFE conditions predicted within the model suggested in Section 2. The results are discussed in Section 4 in terms of the dimensionless parameters of the process introduced in Section 3 after Egorov et al.[44,49]

Two (monodisperse and bidisperse) types of particle size distributions are considered. Although the monodisperse approximation is widely used in modeling, the bidisperse distribution, as a limit of the bimodal distribution, is shown to be more relevant for analysis of the laboratory-scale experimental conditions.[19] This case assumes that "regular" particles of a typical radius, e.g., ~500 μm, and the so-called "dust" particles of a much smaller size, e.g., ~50 μm, are distinguished as the principal fractions in the packed bed. Dust adheres to the surface of the regular particles, not being captured by sieving, and behaves as broken cells. At the same time, the bidisperse structure of a packed bed explains various extraction effects within the framework of the SC approach, in particular, the prolonged initial high-rate extraction stage of SFE, followed by the rapid decrease of the outlet solute concentration.[14,17]

2. MODEL FORMULATION

2.1. Mass Transfer in the Plant Material. The initial content, θ_0, of extractable oil compounds per unit volume of the raw material is assumed to be uniformly distributed over the plant cells. At a given temperature and pressure, the SFE process is controlled by the limiting concentration θ_*[50,51] of the solute saturation in the solvent. Thus, θ_* is a constant that can be

https://dx.doi.org/10.1021/acs.iecr.0c03329
Ind. Eng. Chem. Res. XXXX, XXX, XXX−XXX

calculated based on the available correlations[50,51] or estimated by fitting the model to the experimental data.[19]

The permeability of cell membranes and transport channels controls the rates of internal mass transfer during SFE. The solvent, penetrating into the cells, dissolves the solute up to the saturation concentration θ_*.[10] The dissolved solute diffuses out of the cell across the cell membrane. The system of intercellular space and cell walls that encompasses the cells plays the role of transport channels, where the solute diffuses to the particle surface according to Fick's law with the apparent diffusion coefficient D_{eff}.[49]

Within the framework of the shrinking core (SC) model, it is assumed that the initial oil content is relatively high, i.e., $\theta_0 \gg \theta_*$, and the resistance of the transport channels is the principal factor limiting the internal mass transfer.[13,19,49,52] As a consequence, a sharp concentration front forms, and moves inside every particle of the raw material (Figure 2a). This

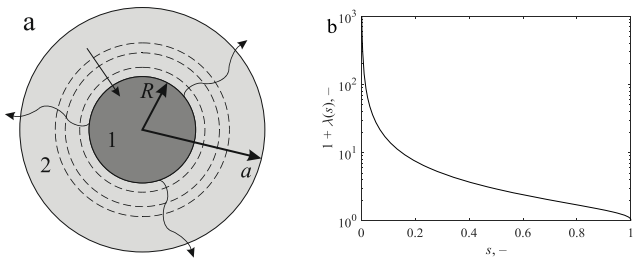

Figure 2. (a) Schematics of the shrinking core model for spherical particles: 1—the oil-containing core, 2—the outer region with the solute diffusing to the particle surface according to Fick's law, a—the particle radius, and R—the current position of the interface (radius of the core). The wavy arrows show the solute diffusion paths and the dashed circles show previous positions of the interface with the decrease of R shown by the arrow. (b) Dependence of dimensionless conductivity $\lambda(s)$ of the outer transport region on the amount of extracted oil s according to eq 2, in $\log_{10}$ scale.

boundary separates the internal oil-containing core (1) from the external oil-depleted transport zone (2). The oil concentration in the core is equal to θ_0, and only the dissolved solute is present in the transport region. The core shrinks with the progress of the extraction as the solute diffuses from the interface to the particle surface. The diffusion in the transport zone is quasi-stationary under the assumptions of the SC model, and the current state of the spherical particle of radius a at any time in the packed bed is characterized by the core radius, $0 \le R(t) \le a$.[53] The particle is exhausted when $R = 0$. Hereinafter, the current volume fraction of the outer, transport region of the particle, i.e., $0 \le s \equiv 1 - (R/a)^3 \le 1$, is also used in model formulation. It is equal to the fraction of oil extracted from the particle.

The local governing equations of the SC model inside the particle were introduced by Goto et al.[13] in terms of R and can be reformulated[19,54] in terms of s as follows

$$\frac{\theta_0}{\theta_*}\frac{\partial s}{\partial t} = \frac{3}{a}q, \quad s|_{t=0} = 0 \tag{1}$$

$$q = \frac{2D_{\text{eff}}}{a}\lambda(s)(1 - c), \quad \lambda(s) = \frac{0.5(1 - s)^{1/3}}{1 - (1 - s)^{1/3}} \tag{2}$$

A detailed derivation of eqs 1 and 2 with the discussion on the diffusive boundary layer around a particle is given in the Supporting Information. Here, $0 \le c \le 1$ is the macroscopic concentration of solute in the pores of the packed bed averaged over a cross section and scaled by θ_*; by definition, $q\theta_*$ is the mass flux of solute per unit area of the particle surface per unit of time. The expression for q, eq 2, assumes that the thickness of the boundary layer is negligible, and the solute concentration at the particle surface is equal to the bulk value c. The complex $2D_{\text{eff}}\lambda(s)/a$ is the apparent conductivity of the outer transport region of the particle, while the $(1 - c)$-factor is the extraction driving force. The conductivity nonlinearly decreases from ∞ to 0 with an increase in s from 0 to 1, as shown in Figure 2b. The dependence of the solute concentration c on time in the packed bed along the vessel is governed on the macro-scale level by the mass-transfer equation discussed in the next section.

2.2. Mass Transfer in the Packed Bed. The coordinate axis z in the extraction column is directed along the flow of the solvent (Figure 1); $z = 0$ corresponds to the inlet cross section, $z = L$ is the outlet cross section, and L is the height of the packed bed. The gravitational effects are not taken into account. The averaged solute concentration $c(z, t)$ is a function of position along the packed bed and time.

The porosity ε of the packed bed is assumed to be uniform and independent of time. The expansion/shrinkage of the raw material is not considered in the present study. This effect was investigated in refs 7, 55, 56. The rate of solvent consumption is typically fixed, and the corresponding macroscopic superficial fluid velocity along the packed bed is v = const.

The specific surface area of ground particles is an important parameter that depends on their size and directly controls the extraction rates.[37,49,57] In turn, the particle volume distribution $F(a)$ is defined via the particle volume density $f(a)$, i.e., $\mathrm{d}F(a) = f(a)\mathrm{d}a$, and $\mathrm{d}F(a)$ is the volume fraction of particles with the size in the interval $[a; a + \mathrm{d}a]$.[5,19] The histogram of particle size distribution can be obtained by the sieve analysis.[58]

Apparently, the mass-transfer velocities of the solute and solvent in packed beds are different, especially under active mass exchange conditions,[20,35] and, following the general concepts of the macro-scale description, discussed above, the deviation of the superficial solute velocity from that of the solvent is conventionally described in terms of the dispersion tensor.[59−62]

With this in mind, the one-dimensional macroscopic mass-transfer equation, which governs the distribution of the solute concentration c along the packed bed, becomes[53,63,64]

$$\varepsilon\frac{\partial c}{\partial t} + v\frac{\partial c}{\partial z} - D_{\text{ax}}\frac{\partial^2 c}{\partial z^2} = 3(1 - \varepsilon)\int_0^{+\infty} q(s, a)\frac{f(a)}{a}\,\mathrm{d}a \tag{3}$$

Here, $q(s, a)$ and $s(z, t, a)$ are the solutions of local problems (1) and (2) for the particle fraction of size a. The source term on the right-hand side of eq 3 describes the mass transfer from the surface of the particle ensemble to the bulk flow.

The boundary conditions for mass-transport eq 3 have been introduced by Danckwerts[65,66] and are used[18] to close the model of solvent filtration through the packed bed

$$vc(0, t) - D_{\text{ax}}\frac{\partial c(0, t)}{\partial z} = 0, \quad -D_{\text{ax}}\frac{\partial c(L, t)}{\partial z} = 0 \tag{4}$$

The initial condition is

$$c(z, 0) = 0 \tag{5}$$

The problem (1)−(5) is the SFE model analyzed below to study and compare different regimes of axial convective dispersion.

https://dx.doi.org/10.1021/acs.iecr.0c03329
Ind. Eng. Chem. Res. XXXX, XXX, XXX−XXX

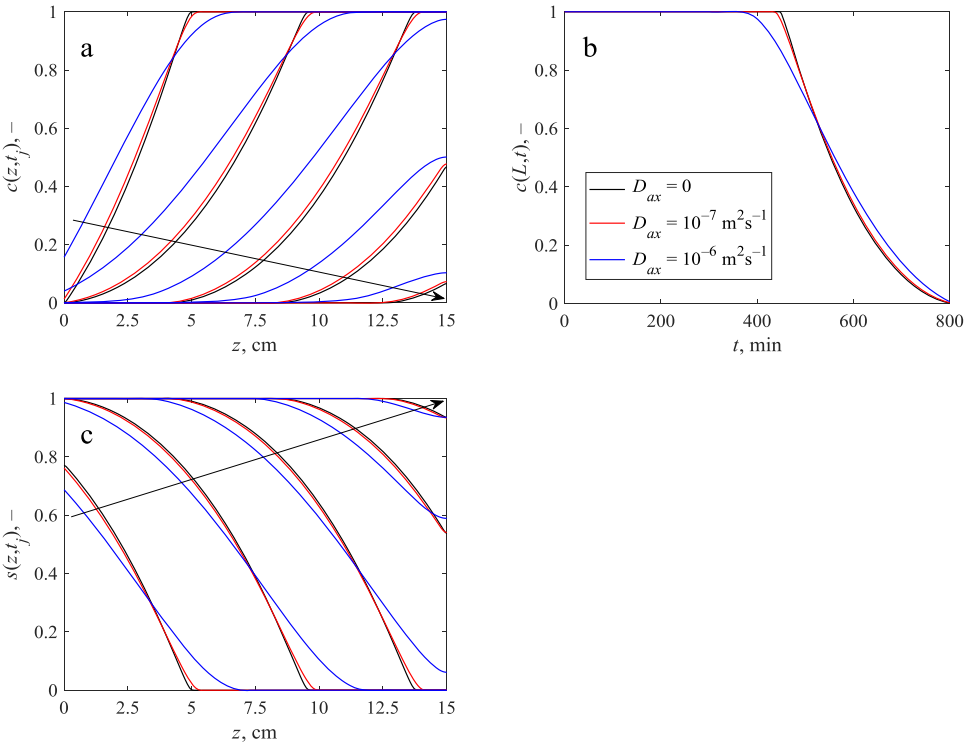

Figure 3. Comparison of three quasi-stationary extraction regimes according to problem (14)−(16) at $\delta_t = 0$ for a packed bed of monodisperse particles, $a = 150$ μm, with and without axial dispersion. Extraction conditions: $L = 15$ cm, $v = 10^{-4}$ m·s^{-1}, $\theta_*/\theta_0 = 0.02625$, $\varepsilon = 0.4$, $D_{\text{eff}} = 10^{-11}$ m^2·s^{-1}, $\delta_{\text{ax}}(a) = \{0; 0.16; 1.6\}$, $\eta(a) = 2.4$, and $Pe_{\text{m}} = 75$ at $D_{\text{m}} = 10^{-9}$ m^2·s^{-1}. See eq 18 for the definitions of $\delta_{\text{ax}}(a)$ and $\eta(a)$. The black curves correspond to the plug flow regime at $D_{\text{ax}} = 0$, the red curves show the dispersion effect at $D_{\text{ax}} = 10^{-7}$ m^2·s^{-1} in accordance with eq 10, and the blue curves show the enhanced dispersion effect at $D_{\text{ax}} = 10^{-6}$ m^2·s^{-1}. (a) Concentration profiles $c(z, t)$ at different time moments, $t = \{80, 240, 400, 560, 720\}$ min, (b) outlet concentration $c(L, t)$, and (c) extracted oil fraction $s(z, t)$ from a given cross section z at time moments corresponding to (a). Arrows show the increase of t from 80 to 720 min at a fixed step of 160 min.

2.3. Overall Extraction Curve and Typical Extraction Time. The so-called overall extraction curve (OEC), $Y(t)$, is the characteristic conventionally observed in experiments. Let $m_0 = (1 - \varepsilon)\theta_0 L$ be the total mass of extractable substances stored in the packed bed per unit area of the bed cross section, and

$$m(t) = v\theta_* \int_0^t c(L, \vartheta)\mathrm{d}\vartheta$$

is the corresponding mass of oil washed out of the packed bed per its cross-sectional unit area by the time moment t. Then, the normalized OEC is defined as

$$Y(t) \equiv \frac{m(t)}{m_0} = \frac{v\theta_*}{(1-\varepsilon)L\theta_0} \int_0^t c(L, \vartheta)\mathrm{d}\vartheta \in [0; 1] \tag{6}$$

On the other hand, OEC is related to the s-function through the mass balance eq 3 and the internal mass-transfer model (1). Integration of eq 3 with respect to z from 0 to L over the packed bed under boundary conditions (4) and substitution of eq 1 yield the following integral−differential relation

$$vc(L, t) = (1 - \varepsilon)\frac{\theta_0}{\theta_*} \int_0^L \int_0^{+\infty} \frac{\partial s}{\partial t} f(a)\mathrm{d}a\ \mathrm{d}z - \varepsilon \int_0^L \frac{\partial c}{\partial t}\mathrm{d}z \tag{7}$$

Further integration of eq 7 with respect to time, using initial conditions (1) and (5), and multiplication by $\theta_*/(1 - \varepsilon)L\theta_0$ result in

$$Y(t) = \frac{1}{L} \int_0^L \int_0^{+\infty} s(z, t, a)f(a)\mathrm{d}a\ \mathrm{d}z - \frac{\varepsilon}{L}\frac{\theta_*}{\theta_0} \int_0^L c(z, t)\mathrm{d}z \tag{8}$$

Thus, from the latter relation, it becomes clear that the oil extracted from the raw material (the first term on the right-hand side) is partly accumulated in pores of the packed bed (the second term on the right-hand side). The ratio θ_*/θ_0 is small in the case of our raw material with high initial oil content, and the last term in eq 8 is hereinafter neglected.

The lower estimate of the time required for the complete extraction of oil from the packed bed is determined by the solvent flow rate. It is obtained if internal resistance and axial dispersion are neglected. Then, $c(z, t)$ is a step function for any t, i.e., $c(L, t) \equiv 1$, during the extraction, and one can easily calculate the minimum time, $t_{\text{total}}^{\min}$, required for the complete extraction with $Y(t_{\text{total}}) = 1$ from eq 6

$$t_{\text{total}}^{\min} = (1 - \varepsilon)\frac{\theta_0}{\theta_*}\frac{L}{v} \tag{9}$$

The duration of a typical laboratory-scale experiment is on the order of $t_{\text{total}}^{\min}$, which is ∼1 h for $\varepsilon = 0.4$, $\theta_0/\theta^* = 5$, $L = 15$ cm, and $v = 10^{-4}$ m·s^{-1}. However, the resistance to solute diffusion along particle transport channels severely affects the total extraction time, and the observed/predicted values of t_{total} are several orders of magnitude larger than $t_{\text{total}}^{\min}$.

https://dx.doi.org/10.1021/acs.iecr.0c03329
Ind. Eng. Chem. Res. XXXX, XXX, XXX−XXX

The time scale given by eq 9 is used hereinafter to plot OECs in dimensionless coordinates. It is equivalent to the use of solvent consumption as an axis since $t/t_{\text{total}}^{\min} \sim vt/L$.

2.4. Correlations for the Axial Dispersion Coefficient in Supercritical CO_2. The heterogeneous systems with "active" and "passive" convection and dispersion are distinguished.[20] The passive dispersion of the solute flow through the porous medium assumes that there are no (chemical or mass exchange) interactions between the phases, and the dispersion tensor depends only on the bed geometric structure. On the contrary, in the case of active dispersion, nonhydrodynamic interactions occur between phases, and the dispersion tensor components may become essentially different.[22] Obviously, SFE is an active dispersion process with mass exchange between the solid phase and the solvent.

Another peculiarity of the SFE phenomenon is that the packed bed is essentially polydisperse, and a spectrum of particle-size inhomogeneity, i.e., $a_1 < a_2 < \cdots < a_n$, should be considered. To the best of our knowledge, there are no reliable estimates for the D_{ax} coefficient obtained directly under SFE conditions of active dispersion in polydisperse beds.

As a consequence, the data available for passive dispersion in supercritical CO_2 flows through monodisperse packed beds of inert particles (glass or sand)[34,45−47] are commonly used in SFE modeling. The widely employed correlations were obtained by Funazukuri et al.[34]

$$D_{\text{ax}} = 1.317\frac{D_{\text{m}}}{\varepsilon}(\varepsilon^2 Pe_{\text{m}})^{1.392} \tag{10}$$

and Yu et al.[46]

$$D_{\text{ax}} = D_{\text{m}}\left(0.58 + 1.65\frac{Pe_{\text{m}}^2}{1 + Pe_{\text{m}}}\right) \tag{11}$$

Here, $Pe_{\text{m}} = vd/\varepsilon D_{\text{m}}$ is the (molecular) Peclet number, D_{m} is the molecular diffusion of solute in the solvent, and d is the representative particle size. From eqs 10 and 11, it becomes clear that the impact of axial dispersion grows nonlinearly with an increase in d, v, and Pe_{m}.

However, the value of d is not well defined in polydisperse systems. The comparison of correlations with the experimental D_{ax} values suggests that the estimates of the axial dispersion coefficient can differ by two to three orders of magnitude. Moreover, the impact of mass transfer on D_{ax} is not fully represented in the available correlations like eqs 10 and 11. Therefore, the sensitivity analysis of the SFE models with respect to uncertainties in the apparent Pe number becomes very challenging.

The values of $D_{\text{m}} = 10^{-9}$ to 10^{-8} m^2·s^{-1}, $d = 10^{-3}$ m, $v = 10^{-5}$ to 10^{-3} m·s^{-1}, and $\varepsilon = 0.4$ typical for SFE conditions are used below in our simulations. The Pe_{m} number spans a wide interval $10 < Pe_{\text{m}} < 10^4$, and $D_{\text{ax}} \sim 10vd$ is independent of D_{m} according to eq 11. Thus, the so-called "mechanical" contribution[46] dominates the molecular diffusion in the fluid flow.

3. SCALE ANALYSIS OF THE SFE PROCESS

3.1. Typical Scales. The typical scales of the SFE process characterize the distribution of the solute concentration along the packed bed (see Figure 3a). It is a sigmoidal curve with its principal part—the extraction zone—bounded by the two "tails" of small, $c \sim 0$, and high, $c \sim 1$, concentration values. The extraction zone where the concentration increases from 0 to 1 initially develops at $z = 0$, and then moves toward $z = L$, leaving the low-concentration region, $c \sim 0$, behind and taking up the high-concentration region, $c \sim 1$. Accordingly, the level of depletion, s, decreases with z; $1 \geq s\,(z = 0) > s\,(z = L) \geq 0$ (see Figure 3c).

The shorter the length of the extraction zone (at fixed L), the higher the efficiency of the SFE process. The concentration curve resembles a step function, and the maximum amount of oil is transported out of the vessel at $c(L, t) = 1$ by the saturated solvent at its highest dissolution capacity and the total extraction time tends to $t_{\text{total}}^{\min}$ given by eq 9. In the case of a wide extraction zone covering the whole length of the SFE vessel, the observed outlet solute concentration decreases, $c(L, t) \ll 1$, and as follows from eq 6, the total extraction time increases with the overall solvent consumption. Thus, the extraction efficiency decreases dramatically as found for packed beds of large particles.

The typical SFE scales correspond to the extraction rates within the concentration front. The spatial scale is $z_{\text{sc}} = \omega t_{\text{sc}}$, where the time scale, $t_{\text{sc}} \neq t_{\text{total}}^{\min}$, being the extraction time of the typical representative particle, is also the time during which the concentration at a given cross section of the packed bed decreases from 1 to 0. The typical velocity, ω, of the concentration front propagation is deduced from eq 9

$$\omega \equiv \frac{L}{t_{\text{total}}^{\min}} = \frac{v}{1 - \varepsilon}\frac{\theta_*}{\theta_0} \ll v \tag{12}$$

Furthermore, integration of eq 1 with respect to time at $c = 0$ from $s(0) = 0$ to $s(t_{\text{sc}}) = 1$ yields[54]

$$t_{\text{sc}}(a_{\text{sc}}) = \frac{\theta_0}{\theta_*}\frac{a_{\text{sc}}^2}{6D_{\text{eff}}}, \qquad z_{\text{sc}}(a_{\text{sc}}) \equiv \omega t_{\text{sc}} = \frac{va_{\text{sc}}^2}{6D_{\text{eff}}(1 - \varepsilon)} \tag{13}$$

where a_{sc} is the apparent particle radius, the representative characteristic of the bed polydispersity.

3.2. Dependence of Extraction Rates on D_{ax}. Figure 3 demonstrates the impact of the axial dispersion on the macroscale concentration distribution (Figure 3a,b) as well as the extracted oil (Figure 3c) in the packed bed compared to the plug flow regime at $D_{\text{ax}} = 0$. The spatial concentration profile flattens and lags in accordance with the diffusion term on the left-hand side of eq 3, while the temporal decrease of concentration starts earlier and slows down with an increase in D_{ax} (the red and blue curves in Figure 3a,b as compared with the black curves). The concentration distribution becomes independent of z in the limit of an ideal mixer, i.e., $c = c(t)$ at $D_{\text{ax}} \to \infty$. In the beginning of the SFE process, the lagging effect (see Figure 3a) is a consequence of the specific boundary condition (4) imposed at $z = 0$. Here, the convective solute transport is essentially counterbalanced by the reversal dispersion flux, and, in the beginning of extraction at the inlet, we have essentially nonzero concentration resulting in reduced driving force of the mass exchange.

The extracted oil concentration profiles shown in Figure 3c reproduce the principal features of the solute distribution, flattening with an increase of D_{ax}values. A crossover point is observed for a set of curves at different D_{ax} corresponding to a fixed time moment. The s-value (the red and blue curves) is greater in the downstream direction and lower in the upstream direction as compared with the case of the plug flow regime (the black curves). Similar behavior can also be observed in the $c(z, t_j)$ curves in Figure 3a. As follows from eq 8, the OECs at different D_{ax} values will not differ much since the area under the $s(z, t_j)$ curves in Figure 3c remain practically the same

https://dx.doi.org/10.1021/acs.iecr.0c03329
Ind. Eng. Chem. Res. XXXX, XXX, XXX−XXX

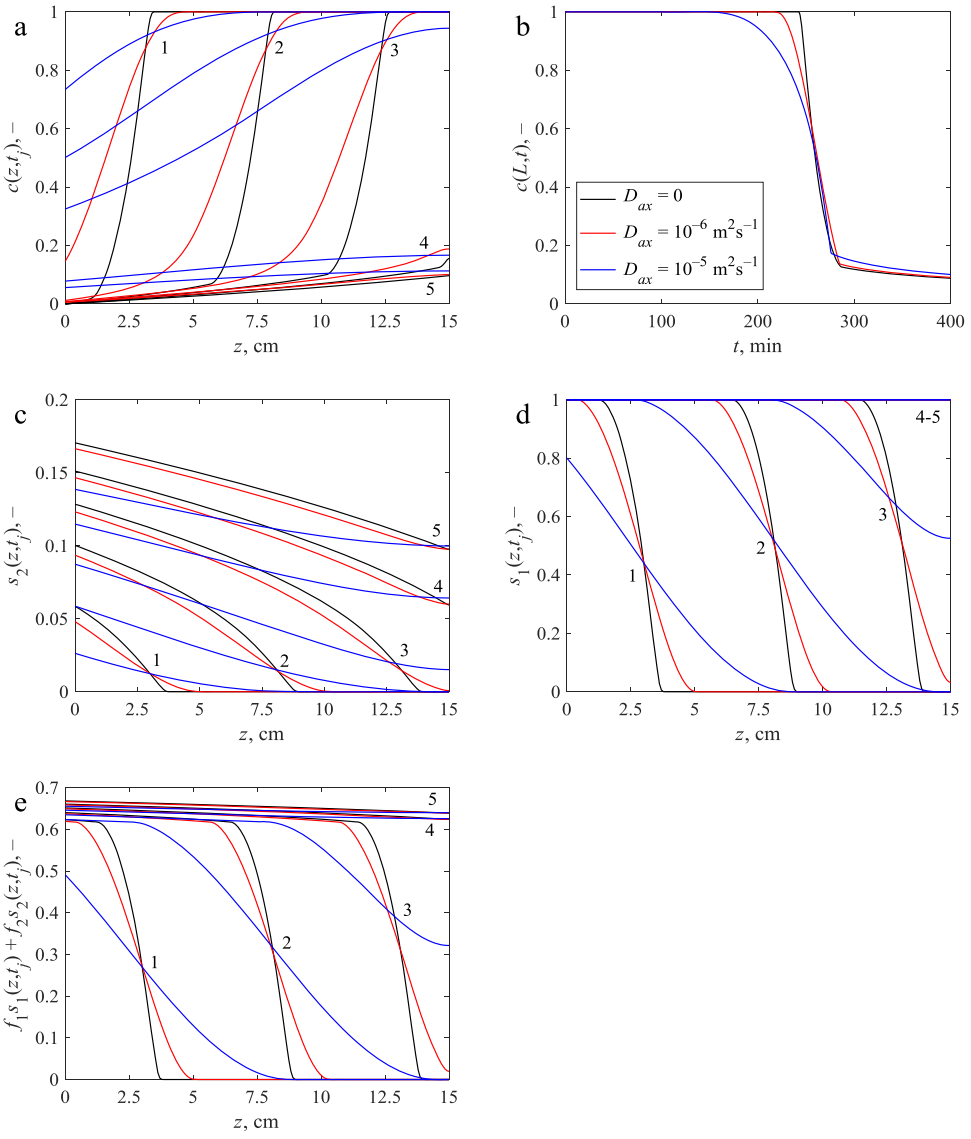

Figure 4. Comparison of three extraction regimes according to eqs 20−22 for a packed bed of bidisperse particles, $a_1 = 15$ μm and $a_2 = 600$ μm at $f_1 = 0.4$, with and without axial dispersion. Extraction conditions: $L = 15$ cm, $v = 10^{-4}$ m·s^{-1}, $\theta_*/\theta_0 = 0.02625$, $\varepsilon = 0.4$, $D_{\text{eff}} = 10^{-12}$ m^2·s^{-1}, $\delta_{\text{ax}}(a_1) = \{0; 1.6; 16\}$, $\eta_1 = 24$, $\eta_2 = 0.15$, and $Pe_{\text{m}} = 300$ at $D_{\text{m}} = 10^{-9}$ m^2·s^{-1}. See text and eq 24 for the definitions of f_1, $\delta_{\text{ax}}(a_1)$, and $\eta_{1,2}$. The black curves correspond to the plug flow regime at $D_{\text{ax}} = 0$, the red curves show the dispersion effect at $D_{\text{ax}} = 10^{-6}$ m^2·s^{-1} in accordance with eq 10, and the blue curves show the enhanced dispersion effect at $D_{\text{ax}} = 10^{-5}$ m^2·s^{-1}. (a) Concentration profiles $c(z, t_j)$ at different time moments, $t_j = \{40, 120, 200, 280, 360\}$ min, $j = 1, 2, 3, 4$, and 5, (b) outlet concentration $c(L, t) = \eta_1 \, dY/d\tau$; (c) oil fraction $s_2(z, t_j)$ extracted from the larger particles at a given cross section z at time moments t_j, (d) oil fraction $s_1(z, t_j)$ extracted from the dust particles, and (e) total extracted oil fraction $f_1 s_1(z, t_j) + f_2 s_2(z, t_j)$. Numbers in (a) and (c−e) next to the curves are the values of subscript j related to the time moments t_j.

independently of D_{ax}. The same conclusion follows from analysis of the $c(L, t)$ curves (Figure 3b), which represent the rate of solute accumulation. It is lower for $D_{\text{ax}} > 0$ before the crossover point $t \sim 550$ min (see Figure 3b). After that, the outlet solute concentration increases with D_{ax} for $t > 550$ min.

3.3. Packed Beds of Monodisperse Particles. To simplify the SFE analysis, it is usually assumed that the particle size distribution is relatively narrow and can be represented, on average, by a single fraction of particles of radius $a_1 = a_{\text{sc}}$ with $f(a) = \delta(a - a_1)$ in eq 3, where δ is the Dirac delta function.[13,52] Problem (1)−(6) take the following dimensionless form

$$\frac{\partial s}{\partial \tau} = \lambda(s)(1 - c), \qquad s|_{\tau=0} = 0 \tag{14}$$

$$\delta_t \frac{\partial c}{\partial \tau} + \frac{\partial c}{\partial \zeta} - \delta_{\text{ax}} \frac{\partial^2 c}{\partial \zeta^2} = \frac{\partial s}{\partial \tau} \tag{15}$$

$$c(0, \tau) - \delta_{\text{ax}} \frac{\partial c(0, \tau)}{\partial \zeta} = 0, \qquad -\delta_{\text{ax}} \frac{\partial c(\eta, \tau)}{\partial \zeta} = 0,$$
$$c(\zeta, 0) = 0 \tag{16}$$

$$Y(\tau) = \frac{1}{\eta} \int_0^{\tau} c(\eta, \tau_1) d\tau_1 = \frac{1}{\eta} \int_0^{\eta} s(\zeta, \tau) d\zeta + O(\delta_t) \tag{17}$$

where $\tau = t/t_{\text{sc}}$ and $\zeta = z/z_{\text{sc}}$ are dimensionless time and spatial coordinates, respectively. The dimensionless complexes are defined as

https://dx.doi.org/10.1021/acs.iecr.0c03329
Ind. Eng. Chem. Res. XXXX, XXX, XXX−XXX

$$\delta_t = \varepsilon\frac{\omega}{v} = \frac{\varepsilon}{1-\varepsilon}\frac{\theta_*}{\theta_0},$$
$$\delta_{ax}(a) = \frac{D_{ax}}{vz_{sc}} = 6(1-\varepsilon)\frac{D_{eff}D_{ax}}{v^2a^2},$$
$$\eta(a) = \frac{t_{total}^{min}}{t_{sc}} = \frac{L}{z_{sc}} = 6(1-\varepsilon)\frac{LD_{eff}}{va^2} \quad (18)$$

Hereinafter, for the monodisperse packed bed, the subscript "1" in particle radius denotation is omitted.

Importantly, δ_t depends only on the oil content and its solubility in the solvent. Its typical value is ~0.01 for pumpkin and sunflower seeds.[19] Thus, the first term in eq 3 and its dimensionless analogues as well as the last term in eqs 8 and 17 can be neglected. Consequently, extraction from the plant material with high initial oil content can be considered as a quasi-stationary process and does not depend on the initial condition (16).

The similarity number $0 < \eta(a) < \infty$ characterizes the efficiency of extraction of the particle fraction of size a. The relative width of the extraction zone tends to zero when $\eta \equiv L/z_{sc}(a) \to \infty$. Thus, $c(\zeta, \tau)$ becomes a steplike function of ζ, on the vessel scale, and the solvent leaving the extraction column is saturated during the entire process. This is the quantitative measure of the efficiency of solvent consumption. For small δ_{ax}, at low axial dispersion, η becomes the only dimensionless parameter that determines the extraction process from monodisperse packed beds.

The complex δ_{ax} is the inverse Peclet number at the spatial scale defined as z_{sc}, generally different from the packed bed height L. In accordance with the above estimates, $D_{ax} \sim 10va$, and for the typical extraction conditions,

$$\delta_{ax} \sim \frac{D_{eff}}{va} \quad (19)$$

Thus, the influence of the axial dispersion on the extraction rates indeed becomes less pronounced with an increase in v and/or a as suggested in.[1,14] At the same time, v and a also determine the width of the extraction zone, and their growth reduces the efficiency of the SFE process with a decrease in the η-number, $\eta \sim v^{-1}a^{-2}$. The significance of the dispersion effect is demonstrated and analyzed quantitatively below in Section 4.

3.4. Packed Beds of Bidisperse Particles. In many cases, two different modes can be distinguished in the particle volume distribution $f(a)$ in ensembles of ground particles.[19] Accordingly, $f(a)$ should be represented, at least, as a sum of two fractions with essentially different modal radii at $a_1/a_2 \sim 0.1$, and $f(a) = f_1\delta(a-a_1) + f_2\delta(a-a_2), f_2 = 1-f_1$. Here, f_1 is the volume fraction of dust particles and, as before, δ is the Dirac delta function. The scale analysis in this case is more challenging since two pairs of scales $\{t_{sc}(a_1); z_{sc}(a_1)\}$ and $\{t_{sc}(a_2); z_{sc}(a_2)\}$ can be introduced; the typical extraction times of individual particles in two fractions can differ by two orders of magnitude, $t_{sc}(a_1) \sim 2.5$ h $\ll t_{sc}(a_2) \sim 5$ d. The total length $z_{sc}(a_2)$ ($\gg z_{sc}(a_1)$) of the extraction zone is determined by the second fraction of the bigger particles, a_2, with $0 < s_2 \equiv s(a_2) < 1$, which is shown in Figure 4c. The two subzones can be distinguished within the extraction zone in a packed bed of the bidisperse particle ensemble. They correspond to the extraction of the dust fraction, $0 < s_1 \equiv s(a_1) < 1$, shown in Figure 4d and the continued extraction of the bigger particle fraction at $s_1 \equiv 1$. As illustrated by black and red curves in Figure 4a, the highest extraction rates and concentration gradients correspond to the first subregion of incomplete extraction of the smaller, dust, particles. Much smaller concentration gradients are observed in the other subregion, where $0 < c \ll 1$. Furthermore, $t_{sc}(a_1)$ is on the order of duration of typical laboratory-scale experiments, about 2−3 h. Therefore, the set of typical scales $\{t_{sc}; z_{sc}\}$ is related to $a_{sc} = a_1$.

The quasi-stationary analogue of problem (1)−(6) takes the following dimensionless form for the bidisperse particle size distribution

$$\frac{\partial c}{\partial \zeta} - \delta_{ax}(a_1)\frac{\partial^2 c}{\partial \zeta^2} = \frac{\partial s_1}{\partial \tau}f_1 + \frac{\partial s_2}{\partial \tau}(1-f_1) \quad (20)$$

$$c(0,t) - \delta_{ax}\frac{\partial c(0,\tau)}{\partial \zeta} = 0, \quad -\delta_{ax}\frac{\partial c(\eta_1,\tau)}{\partial \zeta} = 0 \quad (21)$$

$$\frac{\partial s_i}{\partial \tau} = \frac{\lambda(s_i)}{\xi_i^2}(1-c), \quad i = 1, 2 \quad (22)$$

$$Y(\tau) = \frac{1}{\eta_1}\int_0^{\tau} c(\eta_1, \sigma)\mathrm{d}\sigma = \frac{1}{\eta_1}\int_0^{\eta_1}(f_1 s_1(\zeta,\tau) + f_2 s_2(\zeta,\tau)) \quad (23)$$

Here, $\zeta = z/z_{sc}(a_1)$ and $\tau = t/t_{sc}(a_1)$ assumed for the bidisperse particle size distribution are based on $t_{sc}(a_1)$ and $z_{sc}(a_1)$, while $\xi_i = a_i/a_{sc}$, $i = 1,2$, are the scaled particle radii. By definition, $\xi_1 = 1$, $\xi_2^2 = \eta_1/\eta_2$, $\eta_i = \eta(a_i)$, and

$$\delta_{ax}(a_1) = 6(1-\varepsilon)\frac{D_{eff}D_{ax}}{v^2a_1^2} \sim \frac{D_{eff}a_2}{va_1^2} \quad (24)$$

Let us note that, in general, the similarity number δ_{ax} is inversely proportional to a_1^2 and reduces to that given by eq 19 at $a_1 \to a_2$. In turn, eq 24 reveals that the two respective time scales a_2/v and a_1^2/D_{eff} of solute convective transport on the particle scale and solute extraction from a single particle may both be of primary importance. This also suggests that the cases of active and passive dispersion may differ essentially since the time scale a_1^2/D_{eff} represents SFE under active dispersion conditions and does not appear in the system with passive dispersion.

The dependence of concentration distribution on D_{ax} observed in Figure 4 is similar to the case of the monodisperse packed bed shown in Figure 3. However, the outlet solute concentration, as a function of time, in Figure 4b at a higher value of $D_{ax} = 10^{-6}$ m^2·s^{-1} closely follows the $c(L,t)$ dependence for the plug flow regime, $D_{ax} = 0$. Figure 4c and d demonstrate the impact of axial dispersion on the extraction of oil from respective particle fractions of radii a_2 and a_1. On the one hand, the dispersion affects the extraction from dust to a much higher degree than the extraction from the fraction of larger particles. On the other hand, the corresponding time frame is relatively small, and the dust fraction in our case is exhausted after $t = 250$ min. Thus, the final yield is provided mostly by the dust particles and, as follows from Figure 4e, is virtually independent of axial dispersion. The sets of curves at $t_j = 280$ and 360 min are hardly distinguishable. This assumes that the OEC is also independent of D_{ax} at $t > 280$ min as follows from equality (23).

In general, the smaller the a_1-value, the steeper the concentration front in Figure 4a and the more efficient the extraction of the dust fraction at $\eta_1 \to \infty$. At the same time, the contribution of the dispersion term to the overall mass balance

https://dx.doi.org/10.1021/acs.iecr.0c03329
Ind. Eng. Chem. Res. XXXX, XXX, XXX−XXX

becomes also more pronounced at $a_1 \to 0$. The interaction of these two effects is studied numerically and discussed below in the next section.

4. RESULTS OF NUMERICAL STUDIES

The results of simulations of the SFE process under different experimental conditions are compared in this section. Series of extraction regimes with respect to the axial dispersion coefficient D_{ax} and the corresponding number δ_{ax} are examined inside the two limiting flow bounds: the plug flow, $\delta_{ax} \to 0$, and the ideal mixer, $\delta_{ax} \to \infty$.[18,37] The measure of the relative deviation $E[Y]$ between the two limits is introduced in terms of the measurable quantity, the overall extraction curve Y,

$$E[Y] = \left| \frac{Y_{p.f.} - Y_{i.m.}}{Y_{p.f.}} \right| \tag{25}$$

where subscripts p.f. and i.m. stand for the OECs corresponding to the plug flow and ideal-mixer flow patterns, respectively.

4.1. Monodisperse Packed Beds. The supercritical fluid extraction of oil from packed beds of plant material with high initial oil content, $\delta_t \to 0$, is a quasi-stationary process. The case of monodisperse particle size distribution is characterized by only two dimensionless numbers: the relative width η of the extraction zone and the Peclet number δ_{ax}, eq 18. The set of OECs at different values of η and δ_{ax} is presented in Figure 5a. The highest extraction rates (driving force) are achieved at $\delta_{ax} \to 0$ for any fixed η (thick solid curves). The extraction rates decrease with an increase in δ_{ax} and tend to a certain limit corresponding to the ideal mixer, $\delta_{ax} \to \infty$ (dashed curves). The two limiting curves do not differ much within the interval $0.01 < \eta < 1$. Thus, we can specifically focus on these two bounds in Figure 5b to examine the $E[Y]$-deviation at fixed η.

The extraction efficiency, i.e., the amount of solvent required to reach a certain level of raw material depletion, at any fixed δ_{ax} in monodisperse beds is controlled by η. At larger η values and a relatively narrow extraction zone (see the set of curves in Figure 5a at $\eta = 1$), the OEC $Y_{p.f.}$ noticeably reduces its slope and deviates from the straight line only for $Y_{p.f.} > 0.8$, and, initially, the outlet solute concentration $c_{p.f.}(L, t)$ is close to unity, the maximum value. However, high concentration gradients and large contact time L/v lead to enhanced (negative) impact of axial dispersion, and the two limiting curves, $Y_{p.f.}$ and $Y_{i.m.}$, diverge during the entire process at $\eta = 1$. This is quantitatively illustrated in Figure 5b. In particular, the black curve at $\eta = 1$ reveals a deviation up to 10−15%.

Importantly, the two bounds, $Y_{p.f.}$ and $Y_{i.m.}$, become closer for the lower η values (see Figure 5a) and tend to each other with time (see Figure 5b). The simulations suggest that the overall effect of axial dispersion on the cumulative extraction rates is not significant for $\eta < 0.1$. For instance, at $\eta = 0.03$ and 0.01 in Figure 5b, $E[Y]$ curves, starting from ∼20%, rapidly decrease to ∼5% at $t/t^{min}_{total} \sim 1$. As a consequence, different flow regimes become indistinguishable on the macroscopic-scale level in terms of cumulative characteristics such as OEC at negligibly small dispersion effects.

The two bounds, $Y_{p.f.}$ and $Y_{i.m.}$, are distinct at larger values of η, above 0.1, and the dispersion significantly affects the extraction rates. However, the total extraction time as well as the overall solvent consumption remain reasonably small for this η interval, $t_{total} < 5t^{min}_{total}$, and are not affected by the dispersion.

At first glance, increased solvent flow rates, i.e., high superficial velocity v, might be thought to reduce the δ_{ax} number in eqs 19 and 24 and suppress the negative dispersion effect on the extraction rates as illustrated by Figure 5a,b. However, this would equally reduce the extraction efficiency η given by eq 18, rendering to zero or making, even, negative the total result. From the figures, it is clear that at the same moments of dimensionless time, which correspond to consumed amounts of solvent, the OECs would not change by more than 10−15% versus δ_{ax}, while the corresponding decrease in η would cause a dramatic decrease in extracted oil. Therefore, the enhanced superficial velocities do not seem to be the right choice to improve the SFE process.

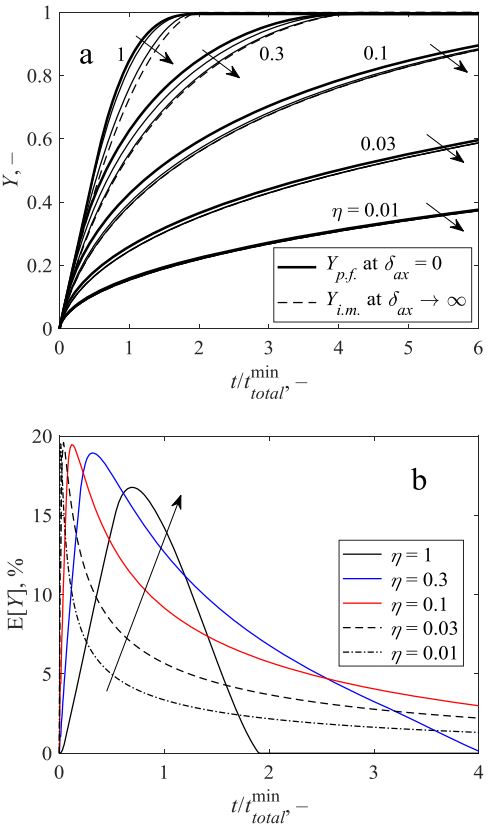

Figure 5. (a) OEC versus the dimensionless time, $t/t^{min}_{total} = \tau/\eta$, at various η and δ_{ax}values. The numbers are the corresponding values of η. The arrows show the increase of δ_{ax}, where the thick curves stand for $Y_{p.f.}$ corresponding to the plug flow, $\delta_{ax} = 0$, and the dashed curves stand for $Y_{i.m.}$ corresponding to the ideal-mixer, $\delta_{ax} \to \infty$, flow patterns. The thin solid curves indicate intermediate regimes at $\delta_{ax} = \{0.1; 1\}$. (b) Relative deviation $E[Y]$ at different η versus the dimensionless time, eq 25. The arrow shows the increase of η according to the legend.

Further, let us note that a typical laboratory-scale scenario (e.g., $L = 20$ cm, $\varepsilon = 0.4$, $d = 2a = 1$ mm, $v = 10^{-4}$ m·s^{-1}, $D_{eff} = 10^{-12}$ m^2·s^{-1}) corresponds to $\eta = 0.03$, $D_{ax} = 2.3\ 10^{-7}$ m^2·s^{-1} (see eq 10), and $\delta_{ax} \sim 10^{-3}$. The η number can be increased up to ∼0.1 for particles of smaller size $d = 0.5$ mm, but this is the lower bound to prevent particle agglomeration and/or channeling in the extractor column. Thus, in accordance with the slopes of OECs in Figure 5a at $\eta < 0.1$, the solute concentration in the entire column tends to zero, the number δ_{ax} does not noticeably affect the OEC, and the $E[Y]$ measure does not exceed 10%, being less than 3−5% for $t/t^{min}_{total} > 1$.

We encounter the same situation in industrial-scale implementations of SFE recently reviewed by del Valle.[12] The lowest production costs are predicted for $L = 3$ m, $a = 1$ mm, and $v = 10^{-2}$ m·s^{-1}. Still, the efficiency of solvent consumption remains very low, with the η number estimated on the order of

https://dx.doi.org/10.1021/acs.iecr.0c03329
Ind. Eng. Chem. Res. XXXX, XXX, XXX−XXX

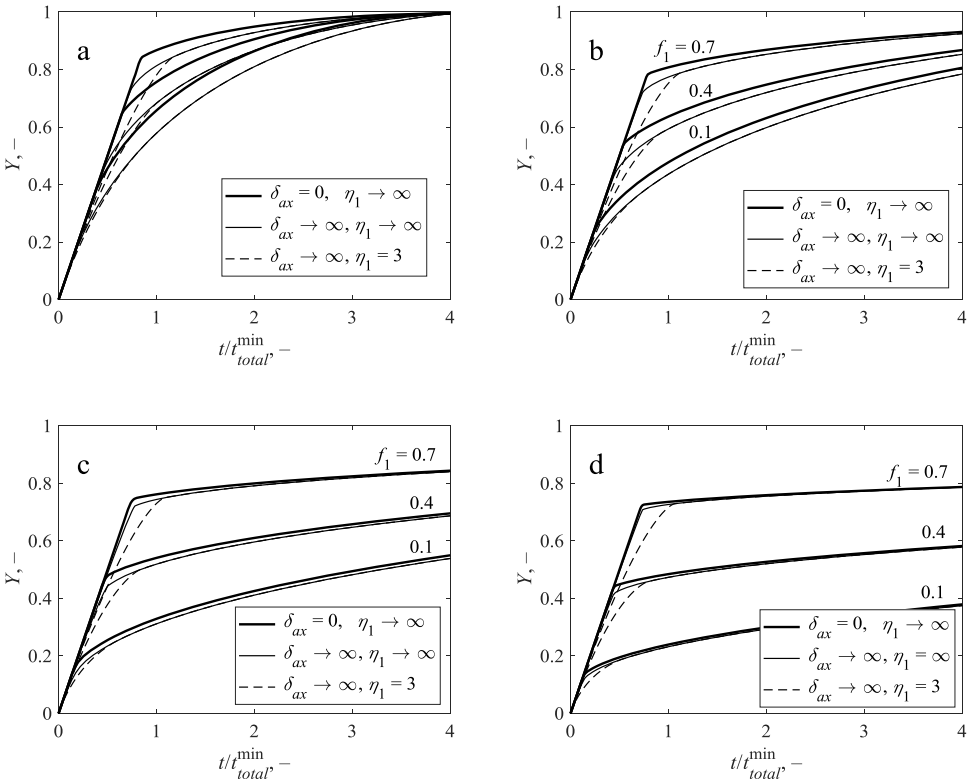

Figure 6. OECs versus the dimensionless time, $t/t^{min}_{total} = \tau/\eta_1$, at different δ_{ax} and η_1 values and (a) $\eta_2 = 0.3$, (b) $\eta_2 = 0.1$, (c) $\eta_2 = 0.03$, and (d) $\eta_2 = 0.01$. The numbers are values of $f_1 = \{0.1; 0.4; 0.7\}$ corresponding to the set of curves.

10^{-3}. The flow regime in the monodisperse packed bed does not play a significant role. In accordance with eq 10, the corresponding "industrial" values of $D_{ax} \sim 10^{-3}$ m^2·s^{-1} result in much lower values $\delta_{ax} \sim 10^{-5}$, and the plug flow approximation of the solution filtration regime with a uniformly small concentration c seems to be the most realistic model scenario in this case.

4.2. Bidisperse Packed Beds. The SC model of a packed bed with a bidisperse particle size distribution, $\{(a_1; f_1), (a_2; 1 - f_1)\}$, allows us to reproduce the SFE kinetics in more detail and with higher accuracy,[19,39] in particular, to study the complex nature of diffusive and convective/dispersive interactions on the particle- and pore-scale levels of the mass-transfer phenomena. The proposed model (20)−(23) for bidisperse beds is equivalent[10] to the Broken-and-Intact Cells (BIC) approach,[17] with the volume fraction f_1 of dust particles effectively substituting for the broken cells. The SFE conditions in this case are fully described by four independent dimensionless numbers: η_1, η_2, $\delta_{ax}(a_1)$, and f_1.

The volume fraction of dust particles f_1 mainly affects the duration of the initial stage of extraction, linear with respect to OEC, as can be seen in Figure 6. The slope of the final nonlinear stage depends on the size of larger particles and flattens with a decrease in η_2. The transition between the two stages is determined by the η_1 value. The transition is abrupt and independent of $\delta_{ax}(a_1)$ at $\eta_1 \to \infty$ (see the solid curves in Figure 6) and becomes smoother at moderate η_1 values (the dashed curves in Figure 6).

As can be seen from eq 24, the value of δ_{ax} strongly depends on the rates of mass exchange between phases during the active dispersion described by the factor D_{eff}/a_1^2. The typical particle size a_1 is assumed to be 20 μm after ref 39. However, the recalculated values of $\delta_{ax}(a_1)$ for the bidisperse packed beds under the laboratory and industrial conditions discussed in the previous Section 4.1 still remain relatively small, being equal to 0.5 and 0.08, respectively. The efficiency of oil extraction from the two fractions is controlled separately by η_1 and η_2. Since η_2 depends solely on a_2, the efficiency of extraction from the larger particles of $d \sim 1$ mm with $\eta_2 \leq 0.1$ on the laboratory scale and $\eta_2 \leq 0.001$ for the industrial-scale conditions does increase in comparison with the monodisperse bed scenario.

The typical values of η_1 for the dust fraction in our case are 1.8 and 2.7 under the laboratory- and industrial-scale conditions, respectively, and Figure 6 illustrates the specific features of OECs for $\eta_1 \sim 3$ (dashed lines) in comparison with the limit of $\eta_1 \to \infty$ (solid lines). A pronounced intermediate stage develops between the initial straight and the final nonlinear part of OEC at moderate η_1 values and high dispersion, $\delta_{ax} \to \infty$. This scenario can hardly be observed in experiments and this shape of OEC is usually associated with the effects of oil desorption.

As a rule, the dust fraction or, identically, the free solute of broken cells, substantially contributes to the overall yield at $\eta_2 \to 0$, Figure 6. The transition bend on OECs occurs approximately at $Y \sim f_1$. All OECs, independently of δ_{ax}, become very similar (compare thick and thin solid curves) at $\eta_1 \to \infty$, converging with time, and practically overlap at $\eta_2 \leq 0.1$ (see Figure 6b−d). For a moderate volume fraction of dust ($f_1 < 0.5$), the OEC limits of $\delta_{ax} = 0$ and ∞ made overlapping by appropriate correction of the f_1-value. Compare, for instance, the respective thick and thin solid curves at $f_1 = 0.1$ and 0.4 in Figure 6a. Thus, the model (best-fit) estimates of the free oil or dust content f_1 can be noticeably influenced by axial dispersion. Figure 6a illustrates this effect for relatively high $\eta_2 = 0.3$. However, the overall SFE efficiencies, i.e., the total extraction time and solvent consumption, are not affected by the dispersion.

https://dx.doi.org/10.1021/acs.iecr.0c03329
Ind. Eng. Chem. Res. XXXX, XXX, XXX−XXX

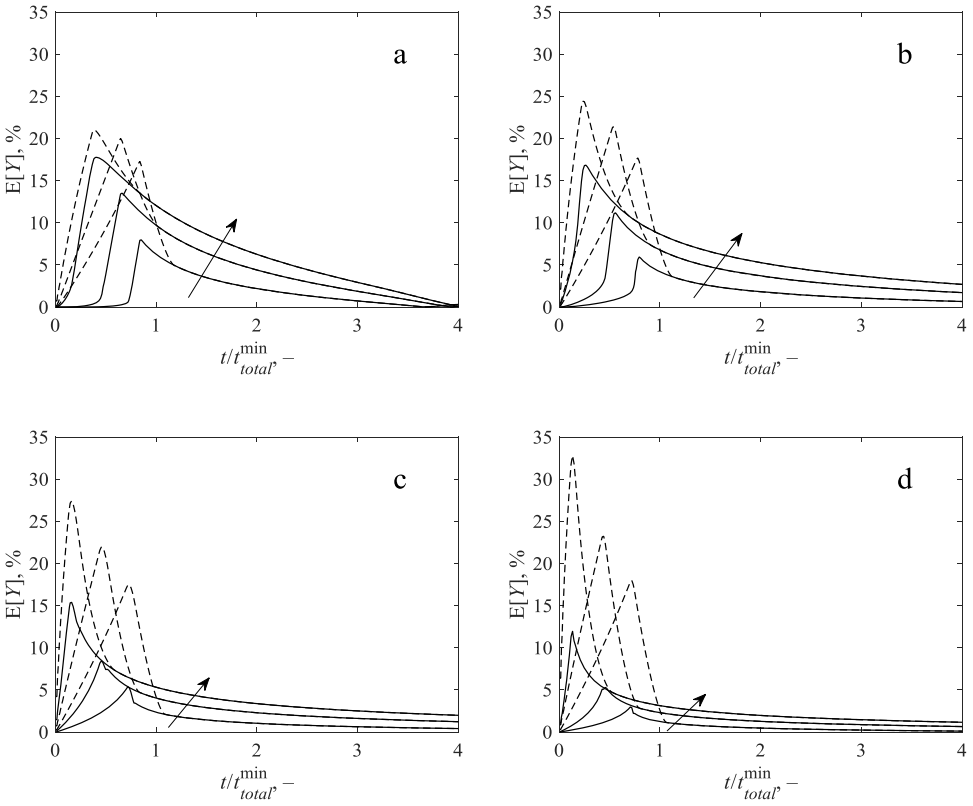

Figure 7. Relative deviation $E[Y]$ versus dimensionless time at different η_2 and f_1 values corresponding to Figure 6. The values $\delta_{ax} = 0$ and $\eta_1 \to \infty$ correspond to $Y_{p.f.}$, while $Y_{i.m.}$ is determined by $\delta_{ax} \to \infty$ and $\eta_1 \to \infty$ for the solid curves and by $\delta_{ax} \to \infty$ and $\eta_1 = 3$ for the dashed curves. (a) $\eta_2 = 0.3$, (b) $\eta_2 = 0.1$, (c) $\eta_2 = 0.03$, and (d) $\eta_2 = 0.01$. The arrows show the increase of $f_1 = \{0.1; 0.4; 0.7\}$.

Uncertainty of OEC prediction related to the axial dispersion is analyzed in Figure 7, where the $Y_{i.m.}$ curves at $\delta_{ax} \to \infty$ and $3 < \eta_1 < \infty$ are compared with the reference $Y_{p.f.}$ curves at $\delta_{ax} = 0$ and $\eta_1 \to \infty$. Figure 7c,d reproduce after Figure 6c,d the laboratory-scale conditions[8,9,67] described by small η_2 values. The maximum of the $E[Y]$ deviation is localized in the region of $t/t^{min}_{total} < 1$, similar to the case of monodisperse packed beds. The difference between two limits diminishes with time for $t/t^{min}_{total} > 1$. Consequently, the axial dispersion, being a crucial phenomenon, manifests itself mainly at the very beginning of the SFE process. Preliminary simulations show that the time of complete extraction does not noticeably depend on δ_{ax}. It should be noted that once the dust fraction is exhausted, $t/t^{min}_{total} > 1$, the discrepancy between the limiting curves, $Y_{p.f.}$ and $Y_{i.m.}$, decreases below 5%, showing the minor importance of axial dispersion.

5. CONCLUSIONS

Supercritical fluid extraction is a complex phenomenon that has not been completely understood so far. The combined effect of interfacial mass exchange and dispersion on the experimentally measurable characteristics, i.e., the overall extraction curve Y, has been examined in the present study. The shrinking core approach is employed to describe the time variation of solute distribution in the plant material. Two approximations of particle size distributions, monodisperse and bidisperse, are considered.

Scale analysis revealed that the extraction conditions for monodisperse distribution are characterized by two dimensionless complexes (similarity numbers), while the bidisperse distribution corresponds to a set of four numbers. The modified Peclet number, $Pe = \delta_{ax}^{-1}$, has been used to analyze the laboratory- and industrial-scale SFE conditions. The typical spatial scale is shown to be the length of the extraction zone in the vessel where the major variation of the solute concentration takes place. This definition reveals the complex nature of interactions of the axial solute dispersion with the interfacial mass exchange in the packed bed.

Analysis of typical laboratory and industrial SFE implementations reveals that, although axial dispersion is always present in the extraction process of packed beds, it does not have a major impact on the total SFE characteristics. From this point of view, the plug flow approximation of the solvent flow can be considered as a reasonably accurate overall description of SFE phenomena on the macro-scale level. The axial dispersion mainly affects the initial phase of extraction characterized by a constant rate. The difference between the overall extraction curves with and without axial dispersion tends to minimum with time and size of larger-particle fraction in the bidisperse packed bed. The OECs do not vary by more than 5−10% for $t/t^{min}_{total} > 1$. Moreover, the total extraction time and total solvent consumption in the limit of relatively small particles are not noticeably affected by dispersion.

An increase of the solvent flow rate was suggested[1,14] earlier as one of the methods to avoid the dispersion. However, it is shown that, at the same time, the superficial velocity also strongly affects the efficiency of the solvent consumption characterized by dimensionless parameters η_i, i = 1,2. As a result, solvent consumption increases dramatically together with the cost of the product.

Future research is needed to examine essential oil extraction. This is a nonstationary process at $\delta_t \sim 1$, and the conventional shrinking core model is no longer applicable. Still, one may

https://dx.doi.org/10.1021/acs.iecr.0c03329
Ind. Eng. Chem. Res. XXXX, XXX, XXX−XXX

expect that the axial dispersion also may not be of high significance under these conditions since, at small initial oil content in the plant material, the solvent is far from the saturation state, and the solute concentration in the pores of the packed bed is thought to be uniformly small. More complex models of the packed bed are of interest as pointed out by Fiori et al.[31] and Sovová et al.[43] Other research challenges originate from the macro-scale heterogeneity caused by stagnant volumes in the bed,[68] and spatial variations of permeability and porosity[1,31,43] with nonuniform radial distributions of superficial velocity.

■ ASSOCIATED CONTENT

Supporting Information

The Supporting Information is available free of charge at https://pubs.acs.org/doi/10.1021/acs.iecr.0c03329.

Derivation of the shrinking core model and analysis of the surface mass-transfer coefficient and the diffusion boundary layer around particles (PDF)

■ AUTHOR INFORMATION

Corresponding Author

Artur A. Salamatin − *Institute of Mechanics and Engineering, FRC Kazan Scientific Center, Russian Academy of Sciences, Kazan 420111, Russia; Institute of Geology and Petroleum Technologies and Institute of Computational Mathematics and Information Technologies, Kazan Federal University, Kazan 420008, Russia;* orcid.org/0000-0002-1099-4016; Email: arthur.salamatin2@gmail.com, salamatin@imm.knc.ru; Fax: +7 (843) 236-52-89

Complete contact information is available at: https://pubs.acs.org/10.1021/acs.iecr.0c03329

Funding

The partial funding due to the Russian Government Program of Competitive Growth of Kazan Federal University is acknowledged.

Notes

The author declares no competing financial interest.

■ ACKNOWLEDGMENTS

This study was supported by the Russian Foundation for Basic Research through grant no. 19-31-60013 and partially through grant no. 18-41-160001.

■ ABBREVIATIONS USED

a	radius of the spherical particle of the ground raw material;
Bi	mass-transfer Biot number, $Bi = a\beta/D_{\text{eff}}$;
c	dimensionless macroscopic solute concentration in the pores of the packed bed averaged over a cross section
d	representative particle diameter for the packed bed;
D_{ax}	streamwise, axial, or longitudinal dispersion coefficient;
D_{eff}	apparent coefficient of solute diffusion along the transport channels of the plant material;
D_{m}	molecular diffusion coefficient of solute in the bulk solvent;
f_i	mass fraction of the ith particle fraction;
L	height of the packed bed and the extraction vessel;
n	number of fractions of particles in the packed bed with distinct typical size;
Pe_{m}	molecular diffusion-based Peclet number, $Pe_{\text{m}} = vd/\varepsilon D_{\text{m}}$;
Sh	Sherwood number, $Sh = a\beta/D_{\text{m}}$;
q	mass flux of solute per unit area of the particle surface per unit of time, normalized by θ_*;
r	radial coordinate in the particle with $r = 0$ corresponding to the particle center;
R	radius of the sharp interface in the particle;
s	fraction of oil extracted from the particle of raw material;
t	time;
v	solvent superficial velocity;
Y	mass fraction of oil extracted from the packed bed to the time moment t;
z	coordinate of cross section of the extraction column with the $z = 0$ corresponding to the inlet cross section;
β	mass-transfer coefficient at the particle surface;
δ_{ax}	dimensionless complex, $\delta_{\text{ax}}(a) = 6(1-\varepsilon)\frac{D_{\text{eff}}D_{\text{ax}}}{v^2a^2}$;
δ_t	dimensionless complex, $\delta_t = \frac{\varepsilon}{1-\varepsilon}\frac{\theta_*}{\theta_0}$;
η	dimensionless complex, $\eta(a) = \frac{L}{z_{\text{sc}}} = 6(1-\varepsilon)\frac{LD_{\text{eff}}}{va^2}$;
ε	porosity of the packed bed;
θ	solute concentration distribution inside the particle;
θ_{s}	solute concentration on the particle surface, $r = a$; the value is close to $c\theta_*$ under SFE conditions;
θ_*	limiting (maximum) solute concentration in the supercritical solvent;
θ_0	oil content of extractable compounds per unit volume of the raw material;
BIC	broken-and-intact cell;
OEC	overall extraction curve;
SC	shrinking core.

■ SUBSCRIPTS

i	index of particle fraction;
sc	typical scale of the process.

■ REFERENCES

(1) Brunner, G.; Baumgartel, H.; Franck, E. U.; Grumbein, W. *Topics in Physical Chemistry - Gas Extraction*; Springer, 1994.

(2) Leung, D. Y. C.; Wu, X.; Leung, M. K. H. A Review on Biodiesel Production Using Catalyzed Transesterification. *Appl. Energy* **2010**, *87*, 1083−1095.

(3) Herrero, M.; Mendiola, J. A.; Cifuentes, A.; Ibáñez, E. Supercritical Fluid Extraction: Recent Advances and Applications. *J. Chromatogr. A* **2010**, *1217*, 2495−2511.

(4) Schütz, E. Supercritical Fluids and Applications − A Patent Review. *Chem. Eng. Technol.* **2007**, *30*, 685−688.

(5) Fiori, L. Supercritical Extraction of Sunflower Seed Oil: Experimental Data and Model Validation. *J. Supercrit. Fluids* **2009**, *50*, 218−224.

(6) Salgın, U.; Döker, O.; Çalimli, A. Extraction of Sunflower Oil with Supercritical CO2: Experiments and Modeling. *J. Supercrit. Fluids* **2006**, *38*, 326−331.

(7) Meyer, F.; Jaeger, P.; Eggers, R.; Stamenic, M.; Milovanovic, S.; Zizovic, I. Effect of CO2 Pre-Treatment on ScCO2 Extraction of Natural Material. *Chem. Eng. Process. Process Intensif.* **2012**, *56*, 37−45.

(8) Salgın, U.; Korkmaz, H. A Green Separation Process for Recovery of Healthy Oil from Pumpkin Seed. *J. Supercrit. Fluids* **2011**, *58*, 239−248.

(9) Özkal, S. G.; Yener, M. E.; Bayındırlı, L. Mass Transfer Modeling of Apricot Kernel Oil Extraction with Supercritical Carbon Dioxide. *J. Supercrit. Fluids* **2005**, *35*, 119−127.

(10) Salamatin, A. A. Detection of Microscale Mass-Transport Regimes in Supercritical Fluid Extraction. *Chem. Eng. Technol.* **2017**, *40*, 829−837.

https://dx.doi.org/10.1021/acs.iecr.0c03329
Ind. Eng. Chem. Res. XXXX, XXX, XXX−XXX

(11) Salamatin, A. A. Numerical scheme for non-linear model of supercritical fluid extraction from polydisperse ground plant material: single transport system. *IOP Conference Series: Materials Science and Engineering*, 2016, Vol. *158*, https://iopscience.iop.org/article/10.1088/1757-899X/158/1/012081/meta.
(12) del Valle, J. M. Extraction of Natural Compounds Using Supercritical CO2: Going from the Laboratory to the Industrial Application. *J. Supercrit. Fluids* **2015**, *96*, 180−199.
(13) Goto, M.; Roy, B. C.; Hirose, T. Shrinking-Core Leaching Model for Supercritical-Fluid Extraction. *J. Supercrit. Fluids* **1996**, *9*, 128−133.
(14) Del Valle, J. M.; De La Fuente, J. C. Supercritical CO2 Extraction of Oilseeds: Review of Kinetic and Equilibrium Models. *Crit. Rev. Food Sci. Nutr.* **2006**, *46*, 131−160.
(15) Oliveira, E. L. G.; Silvestre, A. J. D.; Silva, C. M. Review of Kinetic Models for Supercritical Fluid Extraction. *Chem. Eng. Res. Des.* **2011**, *89*, 1104−1117.
(16) Sovová, H. Rate of the Vegetable Oil Extraction with Supercritical CO2—I. Modelling of Extraction Curves. *Chem. Eng. Sci.* **1994**, *49*, 409−414.
(17) Sovová, H. Broken-and-Intact Cell Model for Supercritical Fluid Extraction: Its Origin and Limits. *J. Supercrit. Fluids* **2017**, *129*, 3−8.
(18) Sovová, H.; Stateva, R. P. Supercritical Fluid Extraction from Vegetable Materials. *Rev. Chem. Eng.* **2011**, *27*, 79−156.
(19) Egorov, A. G.; Salamatin, A. A. Bidisperse Shrinking Core Model for Supercritical Fluid Extraction. *Chem. Eng. Technol.* **2015**, *38*, 1203−1211.
(20) Whitaker, S. *The Method of Volume Averaging*; Springer: Netherlands, 1999.
(21) Quintard, M.; Whitaker, S. One- and Two-Equation Models for Transient Diffusion Processes in Two-Phase Systems. *Adv. Heat Transfer* **1993**, *23*, 369−464.
(22) Quintard, M.; Whitaker, S. Convection, Dispersion, and Interfacial Transport of Contaminants: Homogeneous Porous Media. *Adv. Water Resour.* **1994**, *17*, 221−239.
(23) Howes, F. A.; Whitaker, S. The Spatial Averaging Theorem Revisited. *Chem. Eng. Sci.* **1985**, *40*, 1387−1392.
(24) Coutelieris, F. A.; Delgado, J. M. P. Q. Transport Phenomena in Porous Structures. In *Transport Processes in Porous Media*, Springer-Verlag Berlin: Heidelberg, 2012; pp 39−85.
(25) Han, N.-W.; Bhakta, J.; Carbonell, R. G. Longitudinal and Lateral Dispersion in Packed Beds: Effect of Column Length and Particle Size Distribution. *AIChE J.* **1985**, *31*, 277−288.
(26) Jaćimovski, D.; Garić-Grulović, R.; Vučetić, N.; Pjanović, R.; Bošković-Vragolović, N. Mass Transfer and Concentration Boundary Layer in a Particulate Fluidized Bed. *Powder Technol.* **2016**, *303*, 68−75.
(27) Waslo, S.; Gal-or, B. Boundary Layer Theory for Mass and Heat Transfer in Clouds of Moving Drops, Bubbles or Solid Particles. *Chem. Eng. Sci.* **1971**, *26*, 829−838.
(28) Gal-Or, B. On Motion of Bubbles and Drops. *Can. J. Chem. Eng.* **1970**, *48*, 526−531.
(29) Pfeffer, R. Heat and Mass Transport in Multiparticle Systems. *Ind. Eng. Chem. Fundam.* **1964**, *3*, 380−383.
(30) Pfeffer, R.; Happel, J. An Analytical Study of Heat and Mass Transfer in Multiparticle Systems at Low Reynolds Numbers. *AIChE J.* **1964**, *10*, 605−611.
(31) Fiori, L.; Costa, P. Effects of Differential Permeability on Packed Bed Supercritical Extractors: A Theoretical Insight. *J. Supercrit. Fluids* **2010**, *55*, 176−183.
(32) Huang, Z. Mass Transfer Models for Supercritical Fluid Extraction. In *High Pressure Fluid Technology for Green Food Processing*, Fornari, T.; Stateva, R., Eds.; Springer, 2015; pp 77−115.
(33) Wakao, N.; Funazkri, T. Effect of Fluid Dispersion Coefficients on Particle-to-Fluid Mass Transfer Coefficients in Packed Beds. *Chem. Eng. Sci.* **1978**, *33*, 1375−1384.
(34) Funazukuri, T.; Kong, C.; Kagei, S. Effective Axial Dispersion Coefficients in Packed Beds under Supercritical Conditions. *J. Supercrit. Fluids* **1998**, *13*, 169−175.
(35) Brenner, H. Macrotransport Processes. *Langmuir* **1990**, *6*, 1715−1724.
(36) Sielfeld, C.; del Valle, J. M.; Sastre, F. Effect of Pelletization on Supercritical CO2 Extraction of Rosemary Antioxidants. *J. Supercrit. Fluids* **2019**, *147*, 162−171.
(37) Sovová, H. Steps of Supercritical Fluid Extraction of Natural Products and Their Characteristic Times. *J. Supercrit. Fluids* **2012**, *66*, 73−79.
(38) Sovová, H. Modeling the Supercritical Fluid Extraction of Essential Oils from Plant Materials. *J. Chromatogr. A* **2012**, *1250*, 27−33.
(39) Egorov, A. G.; Salamatin, A. A.; Maksudov, R. N. Forward and Inverse Problems of Supercritical Extraction of Oil from Polydisperse Packed Bed of Ground Plant Material. *Theor. Found. Chem. Eng.* **2014**, *48*, 39−47.
(40) Agarwal, P. K. Transport Phenomena in Multi-Particle Systems—II. Particle-Fluid Heat and Mass Transfer. *Chem. Eng. Sci.* **1988**, *43*, 2501−2510.
(41) Wakao, N.; Funazkri, T. Effect of Fluid Dispersion Coefficients on Particle-to-Fluid Mass Transfer Coefficients in Packed Beds. Correlation of Sherwood Numbers. *Chem. Eng. Sci.* **1978**, *33*, 1375−1384.
(42) Lee, A. K. K.; Bulley, N. R.; Fattori, M.; Meisen, A. Modelling of Supercritical Carbon Dioxide Extraction of Canola Oilseed in Fixed Beds. *J. Am. Oil Chem. Soc.* **1986**, *63*, 921−925.
(43) Sovová, H.; Kučera, J.; Jež, J. Rate of the Vegetable Oil Extraction with Supercritical CO2—II. Extraction of Grape Oil. *Chem. Eng. Sci.* **1994**, *49*, 415−420.
(44) Maksudov, R. N.; Egorov, A. G.; Mazo, A. B.; Aljaev, V. A.; Abdullin, I. S. Mathematical Model of Oil-Bearing Crop Seeds Extraction by Supercritical Carbon Dioxide. *Supercrit. Fluids Theory Pract.* **2008**, *3*, 20−31.
(45) Catchpole, O. J.; Bernig, R.; King, M. B. Measurement and Correlation of Packed-Bed Axial Dispersion Coefficients in Supercritical Carbon Dioxide. *Ind. Eng. Chem. Res.* **1996**, *35*, 824−828.
(46) Yu, D.; Jackson, K.; Harmon, T. C. Dispersion and Diffusion in Porous Media under Supercritical Conditions. *Chem. Eng. Sci.* **1999**, *54*, 357−367.
(47) Tan, C. S.; Liou, D. C. Axial Dispersion of Supercritical Carbon Dioxide in Packed Beds. *Ind. Eng. Chem. Res.* **1989**, *28*, 1246−1250.
(48) Ghoreishi, S. M.; Akgerman, A. Dispersion Coefficients of Supercritical Fluid in Fixed Beds. *Sep. Purif. Technol.* **2004**, *39*, 39−50.
(49) Egorov, A. G.; Mazo, A. B.; Maksudov, R. N. Extraction from a Polydisperse Granular Layer of Milled Oilseeds with Supercritical Carbon Dioxide. *Theor. Found. Chem. Eng.* **2010**, *44*, 642−650.
(50) del Valle, J. M.; de la Fuente, J. C.; Uquiche, E. A Refined Equation for Predicting the Solubility of Vegetable Oils in High-Pressure CO 2. *J. Supercrit. Fluids* **2012**, *67*, 60−70.
(51) del Valle, J. M.; Urrego, F. A. Free Solute Content and Solute-Matrix Interactions Affect Apparent Solubility and Apparent Solute Content in Supercritical CO2 Extractions. A Hypothesis Paper. *J. Supercrit. Fluids* **2012**, *66*, 157−175.
(52) Döker, O.; Salgin, U.; Yildiz, N.; Aydoğmuş, M.; Çalimli, A. Extraction of Sesame Seed Oil Using Supercritical CO2 and Mathematical Modeling. *J. Food Eng.* **2010**, *97*, 360−366.
(53) Egorov, A. G.; Salamatin, A. A. Optimization Problems in a Theory of Supercritical Fluid Extraction of Oil. *Russ. Math.* **2015**, *59*, 48−56.
(54) Salamatin, A. A. Estimation of the Axial Dispersion Effect on Supercritical Fluid Extraction from Bidisperse Packed Beds. *Russ. J. Phys. Chem. B* **2017**, *11*, 1180−1187.
(55) Stamenic, M.; Zizovic, I.; Eggers, R.; Jaeger, P.; Heinrich, H.; Rój, E.; Ivanovic, J.; Skala, D. Swelling of Plant Material in Supercritical Carbon Dioxide. *J. Supercrit. Fluids* **2010**, *52*, 125−133.
(56) Voges, S.; Eggers, R.; Pietsch, A. Gas Assisted Oilseed Pressing. *Sep. Purif. Technol.* **2008**, *63*, 1−14.
(57) Fiori, L.; Basso, D.; Costa, P. Seed Oil Supercritical Extraction: Particle Size Distribution of the Milled Seeds and Modeling. *J. Supercrit. Fluids* **2008**, *47*, 174−181.

https://dx.doi.org/10.1021/acs.iecr.0c03329
Ind. Eng. Chem. Res. XXXX, XXX, XXX−XXX

(58) Fiori, L. Grape Seed Oil Supercritical Extraction Kinetic and Solubility Data: Critical Approach and Modeling. *J. Supercrit. Fluids* **2007**, *43*, 43−54.
(59) Weber, T. W.; Chakravorti, R. K. Pore and Solid Diffusion Models for Fixed-bed Adsorbers. *AIChE J.* **1974**, *20*, 228−238.
(60) Chao, R.; Hoelscher, H. E. Simultaneous Axial Dispersion and Adsorption in a Packed Bed. *AIChE J.* **1966**, *12*, 271−278.
(61) Suzuki, M.; Smith, J. M. Axial Dispersion in Beds of Small Particles. *Chem. Eng. J.* **1972**, *3*, 256−264.
(62) Suzuki, M.; Smith, J. M. Kinetic Studies by Chromatography. *Chem. Eng. Sci.* **1971**, *26*, 221−235.
(63) Salamatin, A. A.; Egorov, A. G. Optimization of Supercritical Fluid Extraction: Polydisperse Packed Beds and Variable Flow Rates. *J. Supercrit. Fluids* **2015**, *105*, 35−43.
(64) del Valle, J. M.; Carrasco, C. V.; Toledo, F. R.; Núñez, G. A. Particle Size Distribution and Stratification of Pelletized Oilseeds Affects Cumulative Supercritical CO2 Extraction Plots. *J. Supercrit. Fluids* **2019**, *146*, 189−198.
(65) Danckwerts, P. V. Continuous Flow Systems. Distribution of Residence Times. *Chem. Eng. Sci.* **1953**, *2*, 1−13.
(66) Pearson, J. R. A. A Note on the "Danckwerts" Boundary Conditions for Continuous Flow Reactors. *Chem. Eng. Sci.* **1959**, *10*, 281−284.
(67) Salgın, U.; Salgın, S.; Ekici, D. D.; Uludağ, G. Oil Recovery in Rosehip Seeds from Food Plant Waste Products Using Supercritical CO2 Extraction. *J. Supercrit. Fluids* **2016**, *118*, 194−202.
(68) Bidner, M. S.; Vampa, V. C. A General Model for Convection-Dispersion-Dynamic Adsorption in Porous Media with Stagnant Volume. *J. Pet. Sci. Eng.* **1989**, *3*, 267−281.

https://dx.doi.org/10.1021/acs.iecr.0c03329
Ind. Eng. Chem. Res. XXXX, XXX, XXX−XXX